Structural relaxation effects on the lowest 4f-5d transition of Ce^{3+} in garnets

Quan Manh Phung,[1] Zoila Barandiarán,[2,3] and Luis Seijo[2,3]

[1]*Department of Chemistry, KU Leuven, Celestijnenlaan 200F, B-3001 Leuven, Belgium*
[2]*Departamento de Química, Universidad Autónoma de Madrid, 28049 Madrid, Spain*
[3]*Instituto Universitario de Ciencia de Materiales Nicolás Cabrera, Universidad Autónoma de Madrid, 28049 Madrid, Spain*

(Dated: December 22, 2014)

The role of structural relaxations on the energy of the lowest $4f-5d$ transition of Ce^{3+} in garnets is studied by means of *ab initio* calculations. This study completes previous studies on the roles of the interactions of the Cerium impurity with its first-neighbors and with the rest of the solid hosts, before the relaxations take place. Periodic boundary conditions density functional theory calculations (DFT) and second-order perturbation theory spin-orbit coupling embedded-cluster wave function theory calculations (WFT) have been performed in the garnets $Y_3Al_5O_{12}$, $Lu_3Al_5O_{12}$, $Y_3Ga_5O_{12}$, $Lu_3Ga_5O_{12}$, and $Ca_3Sc_2Si_3O_{12}$ doped with Ce^{3+}. The local relaxation effects on the $4f-5d$ transition are similar in the WFT and DFT calculations. They produce a blue shift in Al and Ga garnets in which Ce substitutes for smaller Y and Lu cations, which is found to be basically due to the local expansions around the impurity, with only minor contributions from angular relaxations. Atomic relaxations of more distant neighbors enhance the blue shift. Although the embedding effects of the undistorted garnets are known to make the differences between the $4f-5d$ transition in Al and Ga garnets, we find that the structural relaxations are responsible for the small differences between the $4f-5d$ transition in $Y_3Al_5O_{12}$:Ce^{3+} and $Lu_3Al_5O_{12}$:Ce^{3+}, and in $Y_3Ga_5O_{12}$:Ce^{3+} and $Lu_3Ga_5O_{12}$:Ce^{3+}.

Keywords: Ce, YAG, garnets, 4f-5d transitions, ab initio, defect, relaxation

I. INTRODUCTION

Yttrium aluminum garnet $Y_3Al_5O_{12}$ (YAG) doped with Ce^{3+} is a well known phosphor used in energy efficient solid-state white lighting devices based on InGaN blue-LED.[1,2] The facts that its Ce^{3+} $4f\rightarrow5d$ blue absorption is well adapted to the blue-LED emission and its $5d\rightarrow4f$ emission is yellow[3] and can be mixed with residual blue from the LED to produce white light, make the YAG:Ce^{3+} phosphor useful in LED based illumination devices and a widely studied material. The convenience of producing white light warmer than the cool bluish white light so obtained, boosted the search for alternative phosphors with better efficiencies and color-rendering indexes, and, in particular, for new phosphors with red-shifted emission. New Ce^{3+}-doped garnets (with general formula $A_3B'_2B''_3O_{12}$) are on focus in this respect and the search along this line led, for instance, to the discoveries of the $Lu_2CaMg_2Si_3O_{12}$:Ce^{3+} orange phosphor[4] and the $Ca_3Sc_2Si_3O_{12}$:Ce^{3+} green phosphor.[5] Besides illumination, Ce^{3+}-doped garnets find other applications such as scintillation,[6] which is important in medical imaging.

Ab initio calculations can be of great help in the search for new red phosphors because of their ability to pinpoint the factors that govern the light absorptions and emissions. E.g., they have provided an explanation to the fact that the $5d\rightarrow4f$ emission of Ce^{3+} in YAG is blue shifted upon Ga-codoping and red-shifted upon La-codoping, although both codopants produce lattice expansions:[3,7,8] Whereas Ga does not substitute for Al in any preferent site and the lattice expansion it produces lowers the Ce^{3+} $5d$ splitting and shifts the $5d_1$ level to higher energies, La substitutions for Y are more stable near Ce, and the larger La $5p$ and $6s$ orbitals produce an increment of the Pauli repulsion on Ce^{3+}, which increases its $5d$ splitting and shifts its $5d_1$ level to lower energies.[9,10]

Previously, we have shown that the 12 energy levels of the $4f^1$ and $5d^1$ configurations of Ce^{3+} in 21 $A_3B'_2B''_3O_{12}$ garnets of Al, Ga, and Si (B″=Al, Ga, Si), obtained in *ab initio* embedded cluster calculations after a hypothetical *undistorted substitution*, provide useful data and information on differences in these levels between Ce^{3+}-doped garnets and garnet families.[11,12] This is interesting because such calculations simply demand to compute the energy levels of the Ce_A substitutional defect at fixed experimental structures of the undoped garnet hosts, which means avoiding computationally demanding optimizations of the defective solids in the ground and excited states. The two main findings of these two previous *ab initio* studies were the following: Among the six components of the actual D_2 field experienced by Ce^{3+} when it is doped in garnets, only the cubic O_h and tetragonal D_{4h} (ditetragonal-dipyramidal) components lower the $5d_1$-$4f_1$ energy difference significantly.[11] Also, the undistorted host effects play a very important role in the differentiation of the $4f_1\rightarrow5d_1$ transition in different garnet families (of Al, Ga, and Si).[12]

Here, we complete the previous works with an *ab initio* study on the effect of the *structural relaxation* on the lowest Ce^{3+} $4f\rightarrow5d$ transition. This relaxation takes place after Ce^{3+} substitutes for A in the undoped garnet $A_3B'_2B''_3O_{12}$ and creates a Ce_A substitutional defect. Altogether, the undistorted substitution effect and the structural relaxation effect give the total change of a $4f\rightarrow5d$ transition of Ce^{3+} when it is incorporated into the solid host. We study the materials $Y_3Al_5O_{12}$:Ce^{3+}, $Lu_3Al_5O_{12}$:Ce^{3+}, $Y_3Ga_5O_{12}$:Ce^{3+}, and $Lu_3Ga_5O_{12}$:Ce^{3+}, which allow to compare Y/Lu and Al/Ga substitutions, and $Ca_3Sc_2Si_3O_{12}$:Ce^{3+}, which is the only Ce^{3+}-doped normal Si garnet with available $4f\rightarrow5d_1$

experimental data. The results support that the undistorted host effect dominates the differences in $4f$-$5d$ transitions between Ce^{3+}-doped garnet families. Local relaxations are found to provide small corrections that can explain the small $4f$-$5d$ differences in similar materials, like $Y_3Al_5O_{12}$:Ce^{3+} and $Lu_3Al_5O_{12}$:Ce^{3+}.

We give the methodological details in Sec. II, show and discuss the results in Sec. III, and present the conclusions in Sec. IV.

II. METHOD

We performed *ab initio* wave function theory (WFT) embedded cluster calculations with the MOLCAS suite of programs.[13] These are two-step spin-orbit coupling calculations on the $(CeO_8)^{13-}$ cluster. In the first step, we used the many-electron scalar relativistic second-order Douglas-Kroll-Hess (DKH) Hamiltonian.[14,15] We performed state-average complete-active-space self-consistent-field[16–18] (SA-CASSCF) calculations with the active space that results from distributing the open-shell electron in 13 active molecular orbitals with main character Ce $4f, 5d, 6s$. This provided occupied and empty molecular orbitals to feed subsequent multi-state second-order perturbation theory calculations (MS-CASPT2),[19–22] where the dynamic correlation of 73 electrons (the $5s, 5p, 4f, 5d, 6s$ electrons of Ce and $2s, 2p$ electrons of the O atoms) was taken into account. In the second step, spin-orbit coupling effects were included by adding the atomic mean-field integrals (AMFI) approximation of the DKH spin-orbit coupling operator[23] to the Hamiltonian and performing restricted-active-space state-interaction spin-orbit calculations (RASSI-SO)[24] with the previously computed SA-CASSCF wave functions and MS-CASPT2 energies. All the calculations are all-electron, with atomic natural orbital (ANO) relativistic basis sets for Cerium[25] and Oxygen,[26] with respective contractions $(25s22p15d11f4g)/[10s8p5d4f2g]$ and $(14s9p4d3f)/[4s3p2d1f]$. The Hamiltonian of the $(CeO_8)^{13-}$ cluster was supplemented with the *ab initio* model potential (AIMP) embedding Hamiltonians[27] of the $Y_3Al_5O_{12}$, $Lu_3Al_5O_{12}$, $Y_3Ga_5O_{12}$, $Lu_3Ga_5O_{12}$, and $Ca_3Sc_2Si_3O_{12}$ garnets obtained in Refs. 12 and 28 (YAG). These embedding potentials add host electrostatic effects (long-range point-charge Madelung contributions and short-range charge density Coulomb contributions), exchange effects, and Pauli repulsion effects (non-orthogonality contributions due to cluster-host antisymmetry requirements) onto the otherwise isolated cluster. Electron correlation effects between the cluster and the host are excluded from these calculations. The embedding Hamiltonians are made of total-ion embedding AIMPs representing the A, B′, and B″ cations and the O^{2-} anions, which are obtained in self-consistent embedded-ions (SCEI)[29] Hartree-Fock (HF) calculations on the undoped garnets at their experimental structures [160 atom body-centered cubic unit cell (80 atom primitive cell) of the $Ia\bar{3}d$ (230) space group, with 8 formula units of $A_3B'_2B''_3O_{12}$; see Ref. 12 for specific structural data]. They are located at the ionic sites within a cube made of $3\times3\times3$ unit cells and centered on Ce^{3+}, and the embedding potential is completed with a set of $\sim 10^5$ additional point charges situated at lattice sites, generated by the method of Gellé and Lepetit[30] in order to closely reproduce the Ewald potential[31] within the cluster.

In a set of frozen-lattice embedded cluster WFT calculations, experimental ionic sites were used in the 27 unit cells surrounding Ce^{3+} in all the garnets, and the D_2 structures of the $(CeO_8)^{13-}$ clusters were optimized at the spin-orbit level of calculation, RASSI-SO. This was done in the $4f^1$ ground state, $1\Gamma_5$, and in the lowest excited state of the $5d^1$ configuration, $8\Gamma_5$. We used an iterative sequential optimization in specific directions which was stopped when a relative change smaller than 10^{-5} was found in two iterations. The specific directions chosen were the six D_2 totally symmetric displacements of the CeO_8 moiety $S_1 - S_6$ defined in Ref. 12, which are Ce-O bond stretching (S_1, S_2), bond bending (S_3, S_4), and bond twisting (S_5, S_6) D_2 deformations of a reference CeO_8 cube. We calculated the energy differences between the $8\Gamma_5(5d^1)$ and $1\Gamma_5(4f^1)$ states at these structures using the same level of theory, RASSI-SO.

In separate calculations, following the procedure of Ref. 9, we used periodic boundary conditions density functional theory (PBC-DFT) calculations in order to obtain ground state structures of the undoped garnets and of the Ce^{3+}-doped garnets. At the DFT structures of the latter, we computed the energy differences $E[8\Gamma_5(5d^1)] - E[1\Gamma_5(4f^1)]$ using the embedded cluster RASSI-SO WFT method described above. With this DFT-WFT combined procedure, we computed the effects of CeO_8 relaxations and of full lattice relaxations on the Ce^{3+} $4f$-$5d$ energy differences.

The details of the PBC-DFT calculations are the following. We used the Projector Augmented-Wave Method (PAW)[32,33] implemented in the VASP code[34–37] with the generalized gradient approximation (GGA) functional PW91[38], a converged cutoff energy of 520 eV, and a k-point mesh of 4×4×4. For the Ce^{3+}-doped garnets, we used the GGA+U approach[39] with an effective Hubbard parameter for the localized Ce $4f$ of $U_{eff} = 6$ eV, as proposed by Ning *et al.*[40] in $LuAlO_3$:Ce^{3+}. The structures of the undoped garnets were constrained to the $Ia\bar{3}d$ space group. In the Ce^{3+}-doped garnets, Ce substitutes for A at one of the 24(c) unit cell sites with D_2 local symmetry and we used the C222 space group in order to maintain the local symmetry.

III. RESULTS AND DISCUSSION

We have calculated the crystal structures of the undoped garnets $Y_3Al_5O_{12}$, $Lu_3Al_5O_{12}$, $Y_3Ga_5O_{12}$, $Lu_3Ga_5O_{12}$, and $Ca_3Sc_2Si_3O_{12}$ at the PBC-DFT PW91 level. The results are shown in Table I. The theoretical lattice constants show deviations from the experiments of about +1%, which are common in calculations of this type; the largest deviation is +1.1% in $Y_3Ga_5O_{12}$. The theoretical values of the Oxygen

special position parameters, x_O, y_O, z_O, also show deviations under or of around 1%, except 1.5% and 3.3% in the x_O and y_O values of $Y_3Ga_5O_{12}$, and 1.8% and 2.2% in the y_O values of $Y_3Al_5O_{12}$ and $Lu_3Al_5O_{12}$. The good overall agreement suggests that taking an experimental structure or a theoretical structure as a starting point to study structural relaxations around a Ce_A substitutional defect should yield similar results.

In Table II, we summarize the values of the lowest Ce^{3+} $4f$-$5d$ transition $[1\Gamma_5(4f^1)\rightarrow 8\Gamma_5(5d^1)]$, calculated at the RASSI-SO WFT level using different structures for the doped garnets: A) the experimental structure of the undoped garnet; B) the structure resulting from local relaxation of the CeO_8 moiety in RASSI-SO embedded-cluster calculations using the embedding potential of an unrelaxed host with the experimental structure; C) the structure resulting from local relaxation of the CeO_8 moiety in PBC-DFT calculations where the rest of the atoms are fixed at their positions in the experimental structure of the undoped garnet; D) the PBC-DFT structure of the undoped garnet; and E) the structure resulting from full atomic relaxation of the Ce^{3+}-doped garnet in PBC-DFT calculations. The change experienced by the $4f$-$5d$ transition from A to B is the local relaxation effect calculated at the RASSI-SO WFT level, and, from A to C, is the local relaxation effect calculated at the PBC-DFT PW91 level; both effects can be compared. The change from D to E is the full relaxation effect calculated at the PBC-DFT PW91 level. These changes are shown in parentheses in Table II.

We aim at discussing the role of the structural relaxation effect on the $4f$-$5d$ lowest excitation and its comparison with the role of the undistorted host effect. We also aim at linking the relaxation effect with the details of the atomic relaxations; for this, we will use the structures obtained for the CeO_8 moieties, which are given in Tables III and IV. In Table III, we show the D_2 structures of the CeO_8 moiety obtained at different relaxation levels. This structure has 6 degrees of freedom and it is described here in terms of two perpendicular CeO_4 crosses that compose the CeO_8 moiety (Fig. 1): One of them is part of the -A-B$''$O$_4$-A-B$''$O$_4$- tight chains of a $A_3B'_2B''_3O_{12}$ garnet (these chains exist along each cartesian direction of the cubic unit cell);[41] it is called the axial cross and it is shown with red oxygens in Fig. 1, where the chain axis is shown in green. The other CeO_4 cross is perpendicular to the chain axis; it is called the equatorial cross and it is shown with yellow oxygens in Fig. 1. Both crosses are defined in terms of the respective Ce-O distances, d(Ce-O$_a$) and d(Ce-O$_e$), bond angles α_a and α_e, and torsion or dihedral angles ϕ_a and ϕ_e. Deeper insight can be drawn from the structures as described in Table IV, in terms of a reference CeO_8 cube of arbitrary Ce-O distance, e.g. d_{ref}=2.34 Å, and six D_2 distortions S_1 - S_6 (or, equivalently, in terms of a non-arbitrary cube of Ce-O distance d_{cube} and five non-cubic D_2 distortions S_2 - S_6).[11,12] In effect, it was shown in Ref. 11 that, although the six coordinates are important for the sets of seven $4f^1$ and five $5d^1$ levels, the lowest $4f$-$5d$ transition only changes significantly with S_1 and S_3 (or d_{cube} and S_3), which are the O_h breathing of the cube and its the D_{4h} tetragonal distortion (also described as symmetric bond stretching and symmetric bond bending of the two CeO_4 crosses).[11] These two atomic displacement coordinates are shown in the top of Fig. 1. In the bottom of the figure, we show how the energy of the lowest $4f$-$5d$ transition depends on them, according to RASSI-SO calculations on the $(CeO_8)^{13-}$ cluster embedded in a cubic field:[11] shortening the cubic Ce-O distance has the largest impact on the lowering the energy of the lowest $4f$-$5d$ transition; increasing the absolute value of the D_{4h} tetragonal distortion also lowers its energy. This transition energy is basically independent on the remaining atomic displacement coordinates coherent with a D_2 structure: S_2, S_4, S_5, and S_6 (of respective symmetries D_{2h}, D_{2h}, D_4, and D_{2d}, Ref. 11).

In Table II we observe that the structural relaxation effect on the $4f$-$5d$ lowest excitation energy of Ce^{3+}-doped Al and Ga garnets is a blue shift (column E). This blue shift is already produced by the local relaxation of the CeO_8 moiety (columns B and C) and is enhanced by the relaxation of the rest of the host.

Let us discuss the local relaxations. Comparing B and C we see that the local relaxation effects on the $4f$-$5d$ transition are similar in the WFT and DFT calculations, the DFT results leading to slightly higher energies. The local relaxation effect is basically the same in Al and Ga garnets with the same A cation. However, it clearly depends on this cation (its associated blue shift is roughly 500 cm^{-1} higher in Lu garnets than in their Y partners). The latter dependence seems to be responsible for the value of the experimental transition in $Lu_3Al_5O_{12}$:Ce^{3+} being slightly higher than in $Y_3Al_5O_{12}$:Ce^{3+}: the undistorted host calculations give a lower value. The dependence with the A cation is explained with the structural data in Table IV. We only need to analyze the O_h and D_{4h} components of the D_2 structure, S_1 and S_3, if we keep in mind that the values of S_2, S_4, S_5, and S_6 are irrelevant for the lowest $4f$-$5d$ transition.[11] We can observe that the changes in the tetragonal component are small, so that the most important contribution comes from the breathing mode S_1. So, the larger blue shifts of the DFT vs. WFT are just due to their larger values of S_1 or, in other words, to their larger Ce-O distance in their respective reference cubes, d_{cube}. Also, the larger blue shift in Lu garnets vs. Y garnets is just due to their larger d_{cube}. Although d_{cube} is different than the average Ce-O distance in the garnet, $\langle d$(Ce-O)$\rangle$, we can observe in Table III that both of them experience similar changes from garnet to garnet. The positive increments in d_{cube} and $\langle d$(Ce-O)$\rangle$ are measures of the expansion of the O_8 shell when the Ce_A substitutional defect is created and they qualitatively follow the ionic radii mismatch (although they are smaller): +0.17 Å in Ce_{Lu} and +0.12 Å in Ce_Y, using Shannon's 8-fold coordination ionic radii[42] 1.143 Å (Ce^{3+}), 1.019 Å (Y^{3+}), 0.977 Å (Lu^{3+}).

We may recall that EXAFS experiments on Ce^{3+}-doped garnets are able to provide two Ce-O distances,[43] but not the six independent structural parameters of the CeO_8 moiety. This leads us to remark that the facts that the cu-

bic component of the actual D_2 field alone is sufficient to explain the shift of the $4f$-$5d$ transition due to structural relaxations, and that d_{cube} (directly associated to such cubic field) experiences similar changes than the average Ce-O distance $\langle d(\text{Ce-O})\rangle$, suggest that EXAFS data on Ce^{3+}-doped garnets should correlate well with their lowest $4f$-$5d$ transition.

In $Ca_3Sc_2Si_3O_{12}$:Ce^{3+}, the CeO_8 relaxation induces a red shift of the $4f$-$5d$ transition, in opposition to the other garnets. Such shiftt is dominated by the contraction of the O_8 shell, which does not follow the +0.02 Å ionic radii mismatch (Ca^{2+} has a 1.12 Å ionic radius in 8-fold coordination)[42] but is caused by the additional attraction of the oxygens for the positive charge created by the substitution of Ca^{2+} by Ce^{3+}. The WFT calculation leads to a larger contraction than the DFT calculation, and consequently to a larger red shift. In this case, the WFT calculation also gives a larger increment of the absolute value of S_3 than in other cases, which enhances the red shift.

The atomic relaxation beyond the O_8 shell also has an impact on the $4f$-$5d$ excitation: it results from a direct effect and from an indirect effect via the additional relaxation of the O_8 shell it brings. The overall effect can be estimated in DFT calculations as the difference between the DFT full relaxation effect (column E in parentheses) and the DFT local relaxation effect (column C in parenthesis). It means an additional blue shift that amounts 500-800 cm^{-1} and does not have important implications making differences between different garnets. This blue shift enhances the one due to the local relaxations in Al and Ga garnets, and overtakes the local relaxation red shift of $Ca_3Sc_2Si_3O_{12}$:Ce^{3+}. The $4f$-$5d$ blue shift induced by the full relaxation around the Ce_A defect is opposite to the important red shift brought about by the undistorted host effect;[12] however, it does not play an important role at differentiating between garnet families, which seems to be controlled by the undistorted host embedding effects.[12] On the other hand, the relaxation induced blue shifts move the $4f$-$5d$ transitions away from experiments in overall; the higher overall agreement of the undistorted host calculations is the result of a compensation of errors. The fine differences between Ce^{3+}-doped garnets are better reproduced when the structural relaxations are taken into account.

We have also included here (Table V) the results of the RASSI-SO WFT structural optimizations of the CeO_8 moieties in the lowest state of its $5d^1$ configuration, $8\Gamma_5(5d^1)$. These results do not provide information on the role of the relaxation effects compared with the undistorted host effects; they only do on the different relaxation effects in the $4f^1$ ground state and the first $5d^1$ excited state. Comparison of the results with the corresponding B entries in Tables II and III show small changes with respect to the ground state in the angles and in the non-cubic O_8 atomic displacements. The changes in the Ce-O distances, which are shown in parentheses in Table V, are all negative. These bond contractions associated to the lowest $f \rightarrow d$ excitation are known and expected in lanthanide and actinide compounds and materials: They have been reported for the first time in Pa^{4+}-doped Cs_2ZrCl_6 (ref. 44); they have been explained as due to the superposition of three factors (the small relevance of the change in orbital size during the excitation, the ligand field stabilization of the most stable $5d$ orbital, and the larger charge transfer from the ligands to the $4f$ shell in the excited state);[45] and they have been found in all the *ab initio* calculations performed p to date in such materials with the methods used in this paper.[46]

IV. CONCLUSIONS

We have discussed the role of structural relaxations on the lowest $4f$-$5d$ excitation of Ce^{3+}-doped garnets, based on *ab initio* RASSI-SO WFT calculations of the transition energy performed on the $(CeO_8)^{13-}$ cluster under the effects of quantum mechanical embedding potentials of $Y_3Al_5O_{12}$, $Lu_3Al_5O_{12}$, $Y_3Ga_5O_{12}$, $Lu_3Ga_5O_{12}$, and $Ca_3Sc_2Si_3O_{12}$. We used locally relaxed structures calculated at the WFT and DFT levels and globally relaxed DFT structures.

Local relaxation effects on the $4f$-$5d$ transition are similar in the WFT and DFT calculations. They contribute with a blue shift in Ce^{3+}-doped Al and Ga garnets in which Ce substitutes for smaller Y and Lu cations. The angular relaxations do not play a significant role in this blue shift, which is basically due to the local expansion around Ce. The full relaxation of more distant neighbors, which is calculated at the DFT level, enhances the blue shift.

Whereas the embedding effects of the undistorted hosts make the lowest $4f$-$5d$ transition different in different garnet families, the relaxation effects are responsible for the small differences of the transition in closely related garnets where Ce^{3+} substitutes for different cations, like $Y_3Al_5O_{12}$:Ce^{3+} and $Lu_3Al_5O_{12}$:Ce^{3+}.

Acknowledgments

This work was partly supported by a grant from Ministerio de Economía y Competitivad, Spain (Dirección General de Investigación y Gestión del Plan Nacional de I+D+I, MAT2011-24586). QMP thanks the Erasmus Mundus Master in Theoretical Chemistry and Computational Modelling (TCCM) and the Flemish Science Foundation (FWO) for financial support.

[1] S. Nakamura and G. Fasol, *The blue laser diode: GaN based light emitters and lasers* (Springer, Berlin, 1997).

[2] T. Jüstel, H. Nikol, and C. Ronda, Angew. Chem., Int. Ed. **37**,

3084 (1998).
[3] G. Blasse and A. Bril, J. Chem. Phys. **47**, 5139 (1967).
[4] A. A. Setlur, W. J. Heward, Y. Gao, A. M. Srivastava, R. G. Chandran, and M. V. Shankar, Chem. Mater. **18**, 3314 (2006).
[5] Y. Shimomura, T. Honma, M. Shigeiwa, T. Akai, K. Okamoto, and N. Kijima, J. Electrochem. Soc. **154**, J35 (2007).
[6] M. J. Weber, J. Lumin. **100**, 35 (2002).
[7] W. W. Holloway and M. Kestigian, J. Opt. Soc. Am. **59**, 60 (1969).
[8] Y. X. Pan, W. Wang, G. K. Liu, S. Skanthakumar, R. A. Rosenberg, X. Z. Guo, and K. K. Li, J. Alloys Compd. **488**, 638 (2009).
[9] A. B. Muñoz-García and L. Seijo, Phys. Rev. B **82**, 184118 (2010).
[10] A. B. Muñoz-García, J. L. Pascual, Z. Barandiarán, and L. Seijo, Phys. Rev. B **82**, 064114 (2010).
[11] L. Seijo and Z. Barandiarán, Opt. Mater. **35**, 1932 (2013).
[12] L. Seijo and Z. Barandiarán, Phys. Chem. Chem. Phys. **15**, 19221 (2013).
[13] G. Karlström, R. Lindh, P. A. Malmqvist, B. O. Roos, U. Ryde, V. Veryazov, P. O. Widmark, M. Cossi, B. Schimmelpfennig, P. Neogrady, et al., Comput. Mater. Sci. **28**, 222 (2003).
[14] M. Douglas and N. M. Kroll, Ann. Phys. (N.Y.) **82**, 89 (1974).
[15] B. A. Hess, Phys. Rev. A **33**, 3742 (1986).
[16] B. O. Roos, P. R. Taylor, and P. E. M. Siegbahn, Chem. Phys. **48**, 157 (1980).
[17] P. E. M. Siegbahn, A. Heiberg, B. O. Roos, and B. Levy, Phys. Scr. **21**, 323 (1980).
[18] P. E. M. Siegbahn, A. Heiberg, J. Almlöf, and B. O. Roos, J. Chem. Phys. **74**, 2384 (1981).
[19] K. Andersson, P.-A. Malmqvist, B. O. Roos, A. J. Sadlej, and K. Wolinski, J. Phys. Chem. **94**, 5483 (1990).
[20] K. Andersson, P.-A. Malmqvist, and B. O. Roos, J. Chem. Phys. **96**, 1218 (1992).
[21] A. Zaitsevskii and J.-P. Malrieu, Chem. Phys. Lett. **233**, 597 (1995).
[22] J. Finley, P.-A. Malmqvist, B. O. Roos, and L. Serrano-Andrés, Chem. Phys. Lett. **288**, 299 (1998).
[23] B. A. Hess, C. M. Marian, U. Wahlgren, and O. Gropen, Chem. Phys. Lett. **251**, 365 (1996).
[24] P. A. Malmqvist, B. O. Roos, and B. Schimmelpfennig, Chem. Phys. Lett. **357**, 230 (2002).
[25] B. O. Roos, R. Lindh, P. A. Malmqvist, V. Veryazov, and P. O. Widmark, J. Chem. Phys. **112**, 11431 (2008).
[26] B. O. Roos, R. Lindh, P. A. Malmqvist, V. Veryazov, and P. O. Widmark, J. Phys. Chem. A **108**, 2851 (2005).
[27] Z. Barandiarán and L. Seijo, J. Chem. Phys. **89**, 5739 (1988).
[28] J. Gracia, L. Seijo, Z. Barandiarán, D. Curulla, H. Niemansverdriet, and W. van Gennip, J. Lumin. **128**, 1248 (2008).
[29] L. Seijo and Z. Barandiarán, J. Chem. Phys. **94**, 8158 (1991).
[30] A. Gellé and M.-B. Lepetit, J. Chem. Phys. **128**, 244716 (2008).
[31] P. P. Ewald, Ann. Phys. **369**, 253 (1921).
[32] P. E. Blöchl, Phys. Rev. B **50**, 17953 (1994).
[33] G. Kresse and D. Joubert, Phys. Rev. B **59**, 1758 (1999).
[34] G. Kresse and J. Hafner, Phys. Rev. B **47**, 558 (1993).
[35] G. Kresse and J. Hafner, Phys. Rev. B **49**, 14251 (1994).
[36] G. Kresse and J. Furthmüller, Comput. Mat. Sci. **6**, 15 (1996).
[37] G. Kresse and J. Furthmüller, Phys. Rev. B **54**, 11169 (1996).
[38] J. P. Perdew, J. A. Chevary, S. H. Vosko, K. A. Jackson, M. R. Pederson, D. J. Singh, and C. Fiolhais, Phys. Rev. B **46**, 6671 (1992).
[39] S. L. Dudarev, G. A. Botton, S. Y. Savrasov, C. J. Humphreys, and A. P. Sutton, Phys. Rev. B **57**, 1505 (1998).
[40] L. Ning, F. Yang, C. Duan, Y. Zhang, J. Liang, and Z. Cui, J. Phys.: Condens. Matter **24**, 05502 (2012).
[41] A. B. Muñoz-García and L. Seijo, J. Phys. Chem. A **115**, 815 (2011).
[42] R. D. Shannon, Acta Crystallogr. A **32**, 751 (1976).
[43] P. Ghigna, S. Pin, C. Ronda, A. Speghini, F. Piccinelli, and M. Bettinelli, Opt. Mater. **34**, 19 (2011).
[44] L. Seijo and Z. Barandiarán, J. Chem. Phys. **115**, 5554 (2001).
[45] Z. Barandiarán and L. Seijo, J. Chem. Phys. **119**, 3785 (2003).
[46] Z. Barandiarán and L. Seijo, in *Computational Methods in Lanthanide and Actinide Chemistry*, edited by M. Dolg (John Wiley & Sons, New York, 2015).
[47] F. Euler and J. A. Bruce, Acta Crystallogr. **19**, 971 (1965).
[48] A. B. Muñoz-García, E. Anglada, and L. Seijo, Int. J. Quantum Chem. **109**, 1991 (2009).
[49] A. Nakatsuka, A. Yoshiasa, and S. Takeno, Acta Crystallogr. B **51**, 737 (1995).
[50] S. Quartieri, R. Oberti, M. Boiocchi, M. C. Dalconi, F. Boscherini, O. Safonova, and A. B. Woodland, Am. Mineral. **91**, 1240 (2006).
[51] J. M. Ogieglo, A. Zych, K. V. Ivanovskikh, T. Jüstel, C. R. Ronda, and A. Meijerink, J. Phys. Chem. A **116**, 8464 (2012).

TABLE I: Experimental and calculated crystallographic data of the studied garnets: lattice constant a and special position (h) of the $Ia\overline{3}d$ (230) space group x_O, y_O, z_O.

Garnet		a(Å)	x_O	y_O	z_O
$Y_3Al_5O_{12}$	Exp. (ref. 47)	12.000	–0.0306	0.0512	0.1500
	DFT PBE (ref. 48)	12.114	–0.0306	0.0519	0.1491
	DFT PW91 (this work)	12.096	–0.0308	0.0503	0.1490
$Y_3Ga_5O_{12}$	Exp. (ref. 49)	12.273	–0.0274	0.0546	0.1493
	DFT PW91 (this work)	12.403	–0.0278	0.0564	0.1501
$Lu_3Al_5O_{12}$	Exp. (ref. 47)	11.906	–0.0294	0.0537	0.1509
	DFT PW91 (this work)	11.936	–0.0291	0.0525	0.1498
$Lu_3Ga_5O_{12}$	Exp. (ref. 47)	12.188	–0.0252	0.0570	0.1506
	DFT PW91 (this work)	12.263	–0.0254	0.0576	0.1513
$Ca_3Sc_2Si_3O_{12}$	Exp. (ref. 50)	12.250	–0.0400	0.0501	0.1589
	DFT PW91 (this work)	12.363	–0.0400	0.0499	0.1585

TABLE II: Energies of the lowest $4f$-$5d$ transition of Ce^{3+} in several garnets [$1\Gamma_5(4f^1)\rightarrow 8\Gamma_5(5d^1)$, in cm^{-1}] calculated at the RASSI-SO WFT level using different ground state structures, which are indicated. Maxima of the lowest $4f$-$5d$ experimental absorption bands are also given.

		Ground state structure				
		A [a]	B [b]	C [c]	D [d]	E [d]
		Experimental	WFT	DFT	DFT	DFT relaxed
Material	Exp.[Ref.]	undistorted host	relaxed CeO_8 [f]	relaxed CeO_8 [g]	undistorted host	CeO_8 and host [h]
$Y_3Al_5O_{12}:Ce^{3+}$	22000 [3]	22520	23390 (+870)	23640 (+1120)	23310	24960 (+1650)
$Y_3Ga_5O_{12}:Ce^{3+}$	23800 [3]	24450	25290 (+840)	25460 (+1010)	25260	26940 (+1680)
$Lu_3Al_5O_{12}:Ce^{3+}$	22470 [51]	22100	23420 (+1320)	23720 (+1620)	22500	24970 (+2470)
$Lu_3Ga_5O_{12}:Ce^{3+}$		24110	25410 (+1300)	25700 (+1590)	24460	26880 (+2420)
$Ca_3Sc_2Si_3O_{12}:Ce^{3+}$	22200 [5]	24370	21590 (–2780)	24200 (–170)	25010	25690 (+680)

[a] Undistorted garnet with experimental structure.
[b] WFT ground state relaxed structure of the CeO_8 moiety in an unrelaxed host with the experimental structure.
[c] DFT ground state relaxed structure of the CeO_8 moiety in an unrelaxed host with the experimental structure.
[d] Undistorted garnet with DFT calculated structure.
[e] DFT calculated structure after full relaxation of the CeO_8 moiety and the host structure.
[f] WFT local relaxation effect is given in parentheses.
[g] DFT local relaxation effect is given in parentheses.
[h] DFT full relaxation effect is given in parentheses.

TABLE III: Local structure of the CeO_8 moiety in Ce^{3+}-doped garnets (AO_8 moiety in undoped garnets). Taking one of the three perpendicular -A-B″O_4-A-B″O_4- tight chains of a $A_3B'_2B''_3O_{12}$ garnet[41] as a reference, the moiety is made of an axial CeO_4 cross and an equatorial CeO_4 cross (cf. red atoms and yellow atoms in Fig. 1 respectively). d(Ce-O_a) is the Ce-O distance in the axial CeO_4 cross, α_a is the O_{a1}-Ce-O_{a2} angle, and ϕ_a is the dihedral angle between the two planes of the axial cross, O_{a1}-Ce-O_{a2} and O_{a3}-Ce-O_{a4}. d(Ce-O_e), α_e, and ϕ_e are the equivalent quantities of the equatorial cross. $\langle d(\text{Ce-O})\rangle$ stands for the average Ce-O distance; its change upon cluster and full structure relaxations are given in parenthesis. Distances are given in Å and angles in degree.

Structure [a]	d(Ce-O_a)	α_a	ϕ_a	d(Ce-O_e)	α_e	ϕ_e	$\langle d(\text{Ce-O})\rangle$
			$Y_3Al_5O_{12}$:Ce^{3+}				
A	2.303	71.7	35.8	2.432	73.7	23.7	2.368
B	2.375	71.7	40.2	2.451	71.9	20.7	2.413 (+0.045) [b]
C	2.390	72.0	35.9	2.474	73.6	21.1	2.432 (+0.064) [c]
D	2.329	71.9	37.1	2.467	73.7	22.7	2.398
E	2.420	71.3	36.6	2.525	74.4	21.6	2.473 (+0.075) [d]
			$Y_3Ga_5O_{12}$:Ce^{3+}				
A	2.340	73.9	33.1	2.440	75.2	23.1	2.390
B	2.410	72.6	35.7	2.456	73.1	22.0	2.433 (+0.043) [b]
C	2.426	73.8	29.4	2.469	75.6	22.9	2.448 (+0.058) [c]
D	2.363	73.8	31.9	2.459	75.4	23.9	2.411
E	2.460	73.3	30.8	2.525	76.2	23.1	2.493 (+0.082) [d]
			$Lu_3Al_5O_{12}$:Ce^{3+}				
A	2.276	72.3	33.1	2.383	74.3	24.8	2.330
B	2.375	72.0	38.7	2.428	72.3	20.7	2.402 (+0.072) [b]
C	2.389	72.5	33.6	2.451	74.7	21.9	2.420 (+0.090) [c]
D	2.283	72.6	34.5	2.402	74.5	23.6	2.343
E	2.419	71.5	34.3	2.492	75.4	22.2	2.456 (+0.113) [d]
			$Lu_3Ga_5O_{12}$:Ce^{3+}				
A	2.303	74.7	30.3	2.393	76.4	24.4	2.348
B	2.412	73.0	34.5	2.438	73.6	22.0	2.425 (+0.077) [b]
C	2.424	74.3	27.0	2.459	77.2	23.7	2.442 (+0.094) [c]
D	2.318	74.5	29.3	2.399	76.2	25.2	2.359
E	2.453	73.6	27.8	2.511	78.0	23.8	2.482 (+0.123) [d]
			$Ca_3Sc_2Si_3O_{12}$:Ce^{3+}				
A	2.389	64.4	32.4	2.532	69.7	33.4	2.461
B	2.374	61.8	28.2	2.451	66.4	43.5	2.413 (–0.048) [b]
C	2.402	64.9	31.2	2.494	69.7	33.3	2.448 (–0.013) [c]
D	2.412	64.6	32.8	2.556	69.6	33.0	2.484
E	2.448	63.5	33.9	2.542	70.1	32.5	2.495 (+0.011) [d]

[a] The structure labels correspond to Table II.

[b] WFT local relaxation effect (difference between B and A) is given in parentheses.

[c] DFT local relaxation effect (difference between C and A) is given in parentheses.

[d] DFT full relaxation effect (difference between E and D) is given in parentheses.

TABLE IV: Local structure of the CeO_8 moiety in Ce^{3+}-doped garnets (AO_8 moiety in undoped garnets) expressed in terms of a Ce-O distance in a garnet-specific reference CeO_8 cube, d_{cube}, and its D_2 distortions, S_2 - S_6, as defined in Refs. 11 and 12. The values of the O_h breathing distortion from a common reference cube with d_{ref}=2.34 Å, S_1, are also given; note that two valid alternatives to define the oxygen structure of a CeO_8 moiety with D_2 symmetry are: (d_{cube}, $S_1 = 0$, S_2, S_3, S_4, S_5, S_6) and ($d_{cube} = d_{ref}$, S_1, S_2, S_3, S_4, S_5, S_6); note also that $S_1 = \sqrt{8}\left(d_{cube} - d_{ref}\right)$. S_1 and S_3 are illustrated in Fig. 1. Changes of d_{cube} upon cluster and full structure relaxations are given in parenthesis. All quantities are given in Å.

Structure [a]	d_{cube}	(S_1)	S_2	S_3	S_4	S_5	S_6
			$Y_3Al_5O_{12}:Ce^{3+}$				
A	2.339	–0.0019	–0.2094	0.0156	–0.1018	1.0099	–0.1613
B	2.381 (+0.042) [b]	0.1166	–0.1572	–0.0493	–0.0794	1.0409	–0.3098
C	2.405 (+0.066) [c]	0.1830	–0.1537	0.0293	–0.0999	0.9954	–0.2279
D	2.368	0.0805	–0.2295	0.0213	–0.1064	1.0272	–0.2044
E	2.443 (+0.075) [d]	0.2924	–0.1821	0.0294	–0.1512	1.0315	–0.2221
			$Y_3Ga_5O_{12}:Ce^{3+}$				
A	2.363	0.0647	–0.1629	0.1338	–0.0757	0.9876	–0.1440
B	2.405 (+0.042) [b]	0.1832	–0.0989	0.0277	–0.0638	1.0145	–0.2238
C	2.423 (+0.060) [c]	0.2361	–0.0736	0.1628	–0.0784	0.9474	–0.0965
D	2.385	0.1264	–0.1520	0.1421	–0.0751	0.9926	–0.1106
E	2.467 (+0.082) [d]	0.3578	–0.1059	0.1615	–0.1176	0.9935	–0.1097
			$Lu_3Al_5O_{12}:Ce^{3+}$				
A	2.303	–0.1042	–0.1683	0.0555	–0.0866	0.9766	–0.1044
B	2.372 (+0.069) [b]	0.0894	–0.1202	–0.0190	–0.0741	1.0179	–0.2904
C	2.394 (+0.091) [c]	0.1526	–0.1136	0.0844	–0.1063	0.9756	–0.1782
D	2.315	–0.0696	–0.1911	0.0718	–0.0932	0.9876	–0.1457
E	2.428 (+0.113) [d]	0.2488	–0.1279	0.0734	–0.1597	1.0038	–0.1756
			$Lu_3Ga_5O_{12}:Ce^{3+}$				
A	2.322	–0.0520	–0.1378	0.1961	–0.0727	0.9580	–0.0755
B	2.398 (+0.076) [b]	0.1632	–0.0668	0.0579	–0.0626	0.9946	–0.2087
C	2.418 (+0.096) [c]	0.2203	–0.0514	0.2309	–0.0996	0.9294	–0.0389
D	2.333	–0.0194	–0.1209	0.1879	–0.0677	0.9577	–0.0454
E	2.457 (+0.124) [d]	0.3300	–0.0823	0.2354	–0.1508	0.9598	–0.0391
			$Ca_3Sc_2Si_3O_{12}:Ce^{3+}$				
A	2.426	0.2445	–0.1978	–0.3354	–0.1407	1.0895	0.0850
B	2.370 (–0.056) [b]	0.0857	–0.0685	–0.5333	–0.0623	1.1235	0.2844
C	2.415 (–0.011) [c]	0.2129	–0.1240	–0.3151	–0.1266	1.0663	0.0873
D	2.450	0.3110	–0.2016	–0.3358	–0.1405	1.0997	0.0714
E	2.460 (+0.010) [d]	0.3386	–0.1378	–0.3592	–0.1970	1.1087	0.0471

[a] The structure labels correspond to Table II.

[b] WFT local relaxation effect (difference between B and A) is given in parentheses.

[c] DFT local relaxation effect (difference between C and A) is given in parentheses.

[d] DFT full relaxation effect (difference between E and D) is given in parentheses.

TABLE V: Local structure of the CeO_8 moiety in Ce^{3+}-doped garnets in the lowest state of its $5d^1$ configuration ($8\Gamma_5(5d^1)$ or $5d_1$), as calculated at the WFT (RASSI-SO) relaxed CeO_8 level. See captions of Tables III and IV for the meaning of the structural parameters. Distances and atomic displacements $S_1 - S_6$ are given in Å; angles are given in degree. Changes on the cubic Ce-O distances, d_{cube}, and average Ce-O distances, $\langle d(\text{Ce-O})\rangle$, with respect to the corresponding ground state data are given in parentheses.

	$d(\text{Ce-O}_a)$	α_a	ϕ_a	$d(\text{Ce-O}_e)$	α_e	ϕ_e	$\langle d(\text{Ce-O})\rangle$
$Y_3Al_5O_{12}:Ce^{3+}$	2.358	71.3	40.8	2.435	71.0	21.0	2.397 (–0.017)
$Y_3Ga_5O_{12}:Ce^{3+}$	2.396	72.4	36.1	2.439	72.2	22.2	2.418 (–0.016)
$Lu_3Al_5O_{12}:Ce^{3+}$	2.360	71.8	39.1	2.412	71.5	20.9	2.386 (–0.016)
$Lu_3Ga_5O_{12}:Ce^{3+}$	2.399	72.8	34.7	2.420	72.7	22.1	2.410 (–0.016)
$Ca_3Sc_2Si_3O_{12}:Ce^{3+}$	2.350	61.5	29.1	2.432	65.5	44.6	2.391 (–0.022)

	d_{cube}	(S_1)	S_2	S_3	S_4	S_5	S_6
$Y_3Al_5O_{12}:Ce^{3+}$	2.365 (–0.016)	0.0702	–0.1593	–0.0880	–0.0642	1.0413	–0.3138
$Y_3Ga_5O_{12}:Ce^{3+}$	2.389 (–0.016)	0.1394	–0.0967	–0.0071	0.0439	1.0111	–0.2283
$Lu_3Al_5O_{12}:Ce^{3+}$	2.356 (–0.016)	0.0454	–0.1202	–0.0542	–0.0567	1.0155	–0.2927
$Lu_3Ga_5O_{12}:Ce^{3+}$	2.383 (–0.015)	0.1214	–0.0614	0.0258	–0.0404	0.9889	–0.2120
$Ca_3Sc_2Si_3O_{12}:Ce^{3+}$	2.347 (–0.023)	0.0185	–0.0732	–0.5685	–0.0415	1.1335	0.2798

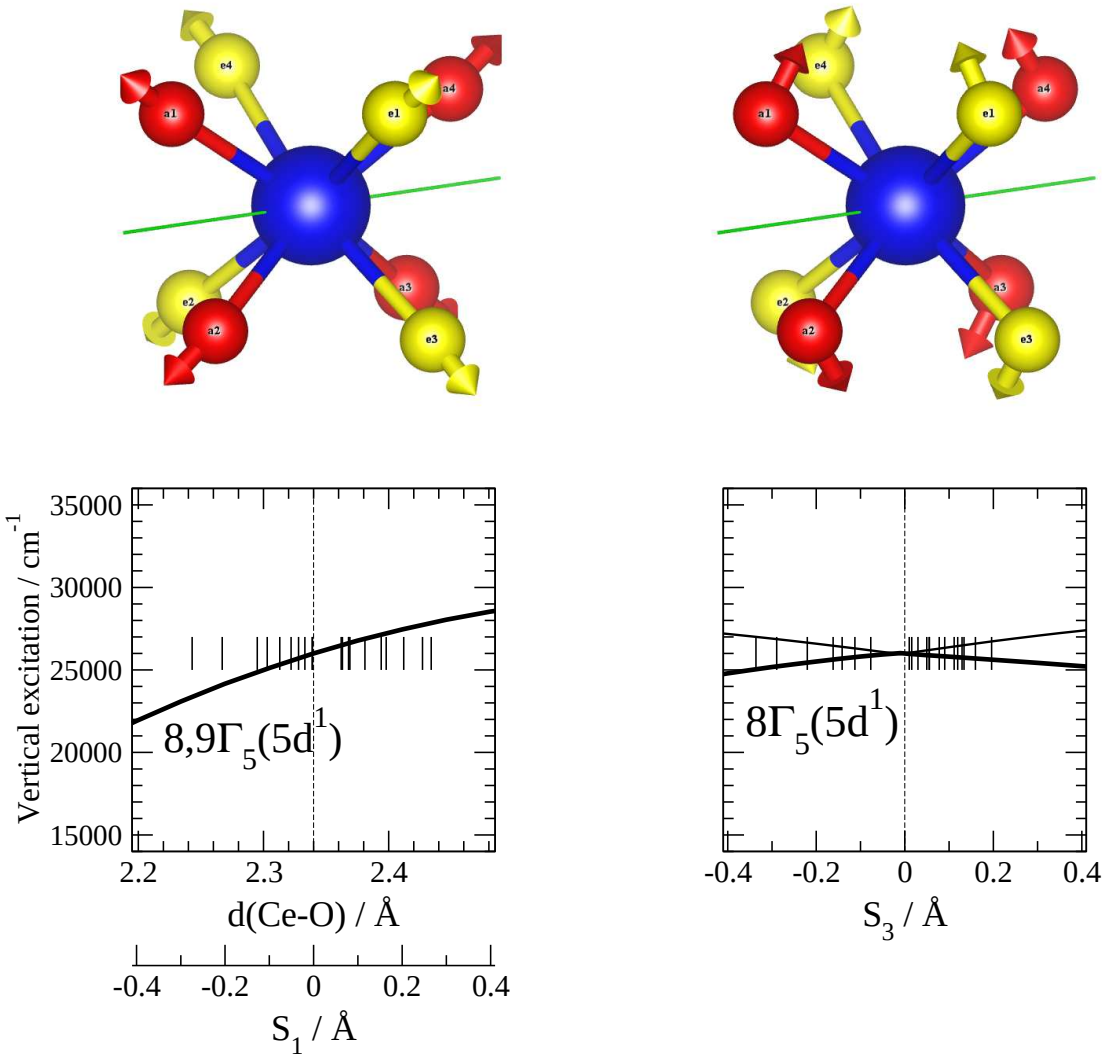

FIG. 1: Top: Cubic O_h breathing (S_1, symmetric bond stretching; left) and tetragonal D_{4h} (S_3, symmetric bond bending; right) atomic displacements which keep the D_2 symmetry of the CeO_8 moiety. The red atoms are the oxygens of the axial CeO_4 cross: along the C_2 symmetry axis that relates O_{a1} with O_{a2} and O_{a3} with O_{a4} (shown in green) lies a tight -A-B"O_4-A-B"O_4- chain of the $A_3B'_2B''_3O_{12}$ garnet.[41] The yellow atoms are the oxygens of the equatorial CeO_4 cross. Bottom: Dependence of the energy of the lowest $4f$-$5d$ transition, $1\Gamma_5(4f^1) \rightarrow 8\Gamma_5(5d^1)$, on the S_1 and S_3 atomic displacements (Ref. 11, RASSI-SO calculations on the $(CeO_8)^{13-}$ cluster embedded in a cubic field).